Journal of Radiation Research, Vol. 63, No. S1, 2022, pp. i21–i25
https://doi.org/10.1093/jrr/rrac023
Supplement Article

Microdistribution of internal radiation dose in biological tissues exposed to ^{56}Mn dioxide microparticles

Valeriy Stepanenko[1,*], Andrey Kaprin[2], Sergey Ivanov[1], Peter Shegay[2], Viktoria Bogacheva[1], Hitoshi Sato[3], Kazuko Shichijo[4], Shin Toyoda[5], Noriyuki Kawano[6], Megu Ohtaki[7], Nariaki Fujimoto[7], Satoru Endo[8], Nailya Chaizhunusova[9], Dariya Shabdarbaeva[9], Kassym Zhumadilov[10] and Masaharu Hoshi[7]

[1]A. Tsyb Medical Radiological Research Center – Branch of the National Medical Research Radiological Center of the Ministry of Health of the Russian Federation, Koroleva Str., 4., Obninsk, Kaluga Region 2490036, Russian Federation
[2]National Medical Research Radiological Center of the Ministry of Health of the Russian Federation, Koroleva Str., 4., Obninsk, Kaluga Region 2490036, Russian Federation
[3]Ibaraki Prefectural University of Health Sciences, 4669-2, Ami-chyo Ami, Inashiki-gun, Ibaraki 300-0394, Japan
[4]Atomic Bomb Disease Institute, Nagasaki University, 1-12-4, Sakamoto, Nagasaki 852-8523, Japan
[5]Department of Applied Physics, Okayama University of Science, 1-1 Ridai, Kita-ku, Okayama 700-0005, Japan
[6]The Center for Peace Hiroshima University, Higashisenda-machi 1-1-89, Naka-ku, Hiroshima 730-0053, Japan
[7]Research Institute for Radiation Biology and Medicine Hiroshima University, 1-2-3, Kasumi, Minami-ku, Hiroshima 734-8551, Japan
[8]Graduate School of Advanced Science and Engineering, Hiroshima University, 1-4-1, Kagamiyama, Higashi, Hiroshima 739-8527, Japan
[9]Semey State Medical University, Abay Str., 103, Semey, 071400, Kazakhstan
[10]Eurasian National University named after L.N. Gumilyov, Munaipasova Str. 13, Astana 010008, Kazakhstan
*Corresponding author. A. Tsyb Medical Radiological Research Center – Branch of the National Medical Research Radiological Center of the Ministry of Health of the Russian Federation, Koroleva Str., 4., Obninsk, Kaluga Region 2490036, Russian Federation, Tel.: +7 (8439) 97002, E-mail address: valerifs@yahoo.com
(Received 3 November 2021; revised 10 April 2022; editorial decision 17 April 2022)

ABSTRACT

Manganese-56 (^{56}Mn) was one of the dominant neutron-activated radionuclides during the first hours following the atomic-bombing of Hiroshima and Nagasaki. The radiation spectrum of ^{56}Mn and the radiation emission from excited levels of ^{56}Fe following ^{56}Mn beta-decay include gamma-quanta, beta-particles, Auger electrons and X-rays. The dispersion of neutron activated ^{56}Mn in the air can lead to entering of radioactive microparticles into the lungs. The investigation of spatial microdistribution of an internal dose in biological tissue exposed to ^{56}Mn is an important matter with regards to the possible elevated irradiation of the lung alveoli and alveolar ducts. The Monte Carlo code (MCNP-4C) was used for the calculation of absorbed doses in biological tissue around ^{56}Mn dioxide microparticles. The estimated absorbed dose has a very essential gradient in the epithelium cells of lung alveoli and alveolar duct: from 61 mGy/decay on the surface of simple squamous cells of epithelium to 0.15 mGy/decay at distance of 0.3 μm, which is maximal cell thickness. It has been concluded that epithelial cells of these pulmonary microstructures are selectively irradiated by low-energy electrons: short-range component of beta-particles spectrum and Auger electrons. The data obtained are important for the interpretation of biological experiments implementing dispersed neutron-activated ^{56}Mn dioxide powder.

Keywords: A-bombing; internal irradiation; ^{56}Mn radioactive microparticles; lungs; alveoli; radiation dose microdistribution

INTRODUCTION

The radionuclide ^{56}Mn ($T_{1/2}$ = 2.58 h) was one of the dominant neutron activated emitters during the first hours following the neutron irradiation as a result of A-bombing of Hiroshima and Nagasaki [1–6]. The radiation spectrum of ^{56}Mn and radiation from excited levels of ^{56}Fe following ^{56}Mn beta-decay, include gamma-quanta, beta-particles, Auger electrons and x-rays [7]. Dispersion of ^{56}Mn dioxide in the air in a form of dust can lead to entering of radioactive microparticles into the lung's alveolar duct and alveoli, when the dispersed powder of this material is inhaled. Taking into account the existence of short-range component of beta-spectrum and electrons as a result of ^{56}Mn decays and radiation from excited levels of ^{56}Fe, the investigation of spatial micro distribution of internal dose in biological tissue exposed by neutron activated ^{56}Mn dioxide microparticles is important matter with regards to possible elevated exposure of lung's microstructures—in comparison with organ-average internal doses. The data obtained are important for the interpretation of the results from biological experiments using dispersed neutron activated ^{56}Mn powder in experimental animals—rats and mice [6, 8–12].

MATERIAL AND METHODS

The absorbed dose was calculated in spherical layers of biological tissue around the ^{56}Mn microparticle as a function of the radial distance from the surface of the microparticle. The ^{56}Mn microparticle is located in the center of the surrounding spherical layers and assumed to be as an isotropic radioactive spherical source. Average diameter of Mn dioxide microparticles is equal to 3 μm [8, 9, 11, 12]. In such kind of geometry only one parameter is important for calculation of absorbed dose distribution around ^{56}Mn microparticle—it is the radial distance from the surface of radioactive particle. The spatial absorbed dose distribution around ^{56}Mn microparticle was calculated for radial distances from the surface of ^{56}Mn microparticle ranged from 10^{-2} μm to 10^{4} μm (see section Results).

For the calculation of the absorbed dose around ^{56}Mn dioxide microparticles the method of stochastic modeling of the interaction of ionizing radiation with matter (Monte-Carlo code MCNP-4C) [13] was used. It should be specially noted that for electron energies less than 10 keV the dose calculation was performed using information about dose point kernels for low-energy electrons presented in the [14].

Radial distribution of absorbed dose versus the distance to the surface of ^{56}Mn dioxide microparticle, surrounded by biological tissue, was estimated with accounting for all components of radioactive emission of ^{56}Mn. Tables 1–5 show all the components of radioactive emission of ^{56}Mn and from excited levels of ^{56}Fe following ^{56}Mn beta-decay (gamma-rays, beta-particles, Auger electrons and X-rays). The contribution to the absorbed dose from ^{56}Mn beta-particles was calculated for each of 20 energy intervals, which were used as discrete approximation of continuous spectrum of all ^{56}Mn beta-particles (Table 3).

Table 6 shows the typical dimension of lung microstructures [16, 17], which were considered as final sites of ^{56}Mn dioxide microparticle penetration into the lungs, when the neutron-activated Mn dioxide powder is inhaled. It was assumed that as a result ^{56}Mn dioxide microparticles are attached to the epithelium. The density of biological tissue

Table 1. Gamma emission from excited levels of ^{56}Fe following ^{56}Mn beta-decay [15]

Energyof gamma-quanta (MeV)	Intensity (gammas per decay)
0.8468	0.9890
1.0380	0.0004
1.2380	0.0010
1.8110	0.2720
2.1130	0.1430
2.5230	0.0099
2.5980	0.0002
2.6570	0.0065
2.9600	0.0031
3.3700	0.0017

Table 2. Beta-particle emission as a result of ^{56}Mn decays to excited levels of ^{56}Fe [7, 15]

Mean/max energy (MeV)	Intensity (beta-particles per decay)
0.0736 / 0.2502	0.0002
0.0992 / 0.3257	0.0116
0.1905 / 0.5726	0.0004
0.2553 / 0.7356	0.1460
0.3820 / 1.0379	0.2790
0.6364 / 1.6104	0.0006
1.2170 / 2.8487	0.5630

Table 3. Digital version of ^{56}Mn spectrum of all beta-particles approximated by 20 energy intervals of electrons [15]

Intervalsof energy (MeV)	Intensity (particlesper decay)
0.0000–0.1424	1.11E-01
0.1424–0.2848	1.26E-01
0.2848–0.4272	1.21E-01
0.4272–0.5695	1.03E-01
0.5695–0.7119	7.91E-02
0.7119–0.8543	6.12E-02
0.8543–0.9967	4.97E-02
0.9967–1.1391	4.65E-02
1.1391–1.2815	4.66E-02
1.2815–1.4239	4.56E-02
1.4239–1.5663	4.32E-02
1.5663–1.7086	3.96E-02
1.7086–1.8510	3.50E-02
1.8510–1.9934	2.96E-02
1.9934–2.1358	2.37E-02
2.1358–2.2782	1.77E-02
2.2782–2.4206	1.18E-02
2.4206–2.5630	6.63E-03
2.5630–2.7054	2.72E-03
2.7054–2.8477	4.17E-04

Table 4. Auger electron emission from excited levels of ^{56}Fe following ^{56}Mn beta-decay [7]

Electrons	Energy (keV)	Intensity (electrons per 100 decays)	Relative probability
K Auger electrons			
KLL	5.370-5.645	0.0139	1
KLX	6.158-6.400	0.00382	0.274
KXY	6.926-7.105	0.000261	0.0187
L Auger electrons	0.510-0.594	0.0428	3.07

Table 5. X-ray emission from excited levels of ^{56}Fe following ^{56}Mn beta-decay [7]

Energy (keV)	Intensity (photons per 100 decays)	Relative probability
6.39091	0.00295	0.51
6.40391	0.00578	1
7.05804	0.00119	0.206

Table 6. Typical dimension of lung's microstructures [16, 17], which were considered as final sites of ^{56}Mn dioxide microparticles penetration into the lungs

Component	Thickness of epithelium
Alveolar duct	Mostly simple squamous epithelium cells (thickness from 0.05 μm to 0.3 μm)
Alveoli	Each alveoli is lined with simple squamous epithelium cells (from 0.05 μm to 0.3 μm thick) and covered over cells by surfactant (about 0.01 μm thick)

was assumed to be equal to 1 g/cm^3. Composition of soft tissue was taken from ICRP Publication 89 [18].

RESULTS

Manganese dioxide particles were considered as spherical isotropic sources of ionizing irradiation from the ^{56}Mn with activity uniformly distributed across their volume. The absorbed doses around the spherical isotropic sources of ^{56}Mn in biological tissue were calculated inside concentric layers, surrounding the microparticles. As a result, radial distribution of absorbed dose was calculated as a function of the distance from the surface of radioactive microparticles (Figs 1 and 2).

Figure 1 shows that exposure to beta-particles as a result of ^{56}Mn decay and electrons emitted from excited levels of ^{56}Fe following ^{56}Mn beta-decay has a significant distance-dependent gradient effect in the epithelium of lung's alveolar ducts, and in the epithelium of alveoli. Absorbed dose per one unit decay is equal to: 61 mGy/decay on the surface of simple squamous cells of epithelium (at distance 0.01 μm from the surface of ^{56}Mn microparticle, which is located near epithelium); 3.4 mGy/decay at 0.05 μm distance—on a layer of epithelial cells at the minimal thickness of cells; 0.15 mGy/decay at distance

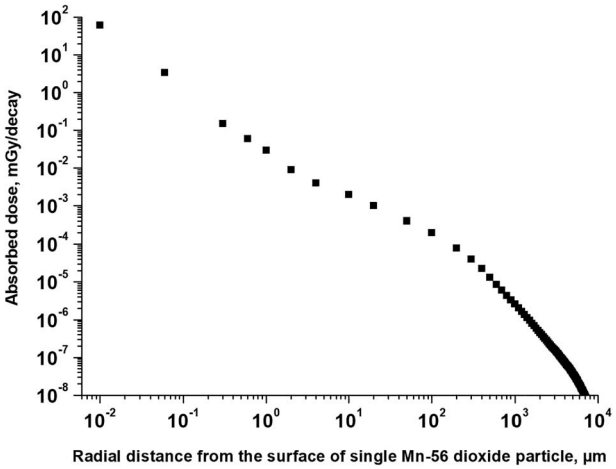

Fig. 1. Radial distribution of absorbed dose versus the distance to the surface of single radioactive ^{56}Mn dioxide microparticle, surrounded by biological tissue: irradiation by beta-particles and electrons.

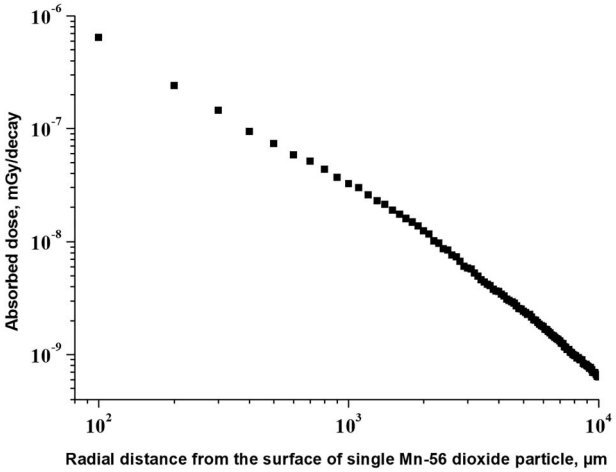

Fig. 2. Radial distribution of absorbed dose versus the distance to the surface of single radioactive ^{56}Mn dioxide microparticle, surrounded by biological tissue: irradiation by photons (gamma-rays and X-rays).

0.3 μm—on a layer of epithelium cells at the maximal thickness of simple squamous cells (see Table 6 with information about thickness of epithelium).

Figure 2 shows that dose from penetrating photon irradiation from the single radioactive ^{56}Mn dioxide microparticle, embedded within the tissue, gives a lower level of irradiation in comparison with irradiation by beta-particles and electrons. At a distance of 100 μm (the diameter of alveolar duct) from the surface of ^{56}Mn dioxide particle, the dose from gammas is equal to 6.4×10^{-7} mGy/decay in comparison with dose 2.1×10^{-4} mGy/decay observed by beta-particle radiation at the same distance. Importantly, that the data shown in Fig. 2 shows the absorbed dose from single radioactive ^{56}Mn dioxide microparticle. The real mean organ dose could be higher—due to penetration of gammas from other ^{56}Mn dioxide microparticles within the lungs.

Nevertheless, the excess dose from beta-particles is estimated about two orders of magnitude higher compared to that from gamma quanta even at a distance of 1000 μm (twice more than diameter of alveoli) from the ^{56}Mn microparticle: 2.5×10^{-6} mGy/decay for beta-particles versus 3.2×10^{-8} mGy/decay for gamma radiation.

DISCUSSION

These data demonstrate that: (i) exposure to beta-particles as a result of ^{56}Mn decay and electrons emission from excited levels of ^{56}Fe following ^{56}Mn beta-decay has a significant distance-dependent gradient in the simple squamous cells of alveoli and alveolar duct epithelium (Fig. 1); and (ii) absorbed dose from penetrating photon irradiation from a radioactive ^{56}Mn dioxide microparticle, embedded in biological tissue, is much less (by 2–3 orders of magnitude) in biological microstructures compared with irradiation by beta-particles and electrons (Figs 1 and 2).

The main contribution to the dose increase at the level of the biological tissue microstructure is due to the low-energy component of the ^{56}Mn beta-particles spectrum, which is the most intense part of this spectrum (top row in Table 3). Some additional contributions to absorbed dose in tissues at very small distances from ^{56}Mn dioxide particles may be due to emitted Auger electrons (Table 4).

From these data it has been concluded that epithelial cells of key pulmonary microstructures are selectively irradiated with short-range beta-spectrum component of ^{56}Mn and with electrons emission from excited levels of ^{56}Fe following ^{56}Mn beta-decay.

These data are important for the interpretation of the results of biological experiments using dispersed neutron-activated ^{56}Mn dioxide powder, which was inhaled by experimental animals—rats and mice [6]. It was demonstrated in these experiments [6] that biological effects caused by internal irradiation from inhaled ^{56}Mn dioxide particles are more significant in comparison to external irradiation by ^{60}Co, despite small values of organ averaged internal radiation doses [10, 11]. The values of organ mean doses in experimental mice and rats are presented in [8, 9, 12].

ACKNOWLEDGEMENT

We express our gratitude to Dr. T. Kolizhenkov, Dr. A. Petukhov, Dr. D. Dubov, Dr. T. Lavrova—the personnel of the A. Tsyb Medical Radiological Research Center – Branch of the National Medical Research Center of Radiology of the Ministry of Health of the Russian Federation, who supported this research in a framework of the Institute Research Program AAAA-A18-118062590091-2 and in a framework of bilateral International Agreement on the scientifical cooperation with Hiroshima University.

CONFLICT OF INTEREST

The authors declare that they have no conflicts of interest.

FUNDING

This work was supported by the Grants-in-Aid for Scientific Research No. 26257501 and 19H01149, KAKENHI to M. Hoshi, Japan.

SUPPLEMENT FUNDING

This work was supported by JSPS KAKENHI Grant Number JP19H01149.

REFERENCES

1. Roesch WC (Ed.). *US-Japan Joint Reassessment of Atomic Bomb Radiation Dosimetry in Hiroshima and Nagasaki (DS86). Final Report. Vol. 1*. Hiroshima: Radiation Effects Research Foundation, 1987 https://www.rerf.or.jp/library/scidata/scids/ds86/ds86aa.html (30 March 2021, date last accessed)
2. Young RW, Kerr GD (Eds). *Reassessment of the Atomic Bomb Dosimetry for Hiroshima and Nagasaki—Dosimetry System 2002 (DS02)*. Hiroshima: Radiation Effects Research Foundation, 2005. https://www.rerf.or.jp/en/library/list-e/scids/ds02-en (25 June 2021, date last accessed)
3. Kerr GD, Egbert SD, Al-Nabulsi I et al. Workshop report on atomic bomb dosimetry—residual radiation exposure: recent research and suggestions for future studies. *Health Phys* 2013;105:140–9.
4. Kerr GD, Egbert SD, Al-Nabulsi I et al. Workshop report on atomic bomb dosimetry – review of dose related factors for the evaluation of exposure to residual radiation at Hiroshima and Nagasaki. *Health Phys* 2015;109:582–600.
5. Weitz R. Reconstruction of beta-particle and gamma-ray doses from neutron activated soil at Hiroshima and Nagasaki. *Health Phys* 2014;107:S43.
6. Hoshi M. A long history exploring radiation exposure. *Impact* 2020:70–2. https://www.ingentaconnect.com/content/sil/impact/2020/00002020/00000003/art00026?crawler=true&mimetype=application/pdf (12 April 2021, date last accessed).
7. Be M-M, Chiste V, Dulieu C et al. *Table of Radionuclides (Vol. 1-a= 1 to 150)*. France: Bureau International des Poids et Mesures. Pavillon de Breteuil, F-92310 Servees, 2004 https://www.bipm.org/utils/common/pdf/monographieRI/Monographie_BIPM-5_Tables_Vol1.pdf (12 April 2021, date last accessed).
8. Stepanenko V, Rakhypbekov T, Otani K et al. Internal exposure to neutron-activated ^{56}Mn dioxide powder in Wistar rats—part 1: dosimetry. *Radiat Environ Biophys* 2016;56:47–54.
9. Stepanenko VF, Rakhypbekov TK, Kaprin AD et al. Irradiation of experimental animals by neutron activated dust: development and realization of the method—first results of international multicenter study. *Radiation and Risk* 2016;25:111–25.

10. Shichijo K, Fujimoto N, Uzbekov D et al. Internal exposure to neutron-activated ^{56}Mn dioxide powder in Wistar rats-part 2: pathological effects. *Radiat Environ Biophys* 2017;56: 55–61.
11. Shichijo K, Takatsuji T, Abishev Zh et al. Impact of local high doses of radiation by neutron activated Mn dioxide powder in rat lungs: protracted pathologic damage initiated by internal exposure. *Biomedicine,* 2020;8:171. doi: https://doi.org/10.3390/biomedicines8060171. https://www.ncbi.nlm.nih.gov/pmc/articles/PMC7345208 (12 April 2021, date last accessed).
12. Stepanenko V, Kaprin A, Ivanov S et al. Internal doses in experimental mice and rats following exposure to neutron-activated $^{56}MnO_2$ powder: results of an international, multicenter study. *Radiat Environ Biophys* 2020;59:683–92.
13. Briemeister JF. *MCNP–A General Monte–Carlo N–Particle Transport Code. Version 4C*. Los Alamos: Los Alamos National Laboratory, 2000.
14. Berger MJ. *Improved Point Kernels for Electron and Beta-Ray Dosimetry*. Washington, DC: Center for Radiation Research, Institute for Basic Standards, National Bureau of Standards; U.S. Atomic Energy Commission, Division of Biomedical and Environmental Research, 1973.
15. RADAR. The decay data. *Available on* . https://www.doseinfo-radar.com/RADARDecay.html 12 April 2021, date last accessed.
16. DukeMedicine. Available on: https://web.duke.edu/histology/NormalBody/Respiratory/Respiratory.html (12 April 2021, date last accessed).
17. Medicalplanet. Available on: https://medicalplanet.su/gistologia/alveoli.html (12 April 2021, date last accessed).
18. Valentin J (Ed). ICRP publication 89. Basic anatomical and physiological data for use in radiological protection reference values. *Ann ICRP,* 2002;32:1–265. https://journals.sagepub.com/doi/pdf/10.1177/ANIB_32_3-4 (12 April 2021, date last accessed)